Quantitative analysis of light scattering in polarization-resolved nonlinear microscopy

Hilton B. de Aguiar, Paulina Gasecka, Sophie Brasselet

Quantitative analysis of light scattering in polarization-resolved nonlinear microscopy

Hilton B. de Aguiar,[1,*] **Paulina Gasecka**[1] **and Sophie Brasselet**[1,2]

[1]*Aix-Marseille Université, CNRS, Centrale Marseille, Institut Fresnel UMR 7249, 13013 Marseille, France*

[2]*sophie.brasselet@fresnel.fr*

[*]*h.aguiar@fresnel.fr*

Abstract: Polarization resolved nonlinear microscopy (PRNM) is a powerful technique to gain microscopic structural information in biological media. However, deep imaging in a variety of biological specimens is hindered by light scattering phenomena, which not only degrades the image quality but also affects the polarization state purity. In order to quantify this phenomenon and give a framework for polarization resolved microscopy in thick scattering tissues, we develop a characterization methodology based on four wave mixing (FWM) process. More specifically, we take advantage of two unique features of FWM, meaning its ability to produce an intrinsic in-depth local coherent source and its capacity to quantify the presence of light depolarization in isotropic regions inside a sample. By exploring diverse experimental layouts in phantoms with different scattering properties, we study systematically the influence of scattering on the nonlinear excitation and emission processes. The results show that depolarization mechanisms for the nonlinearly generated photons are highly dependent on the scattering center size, the geometry used (epi/forward) and, most importantly, on the thickness of the sample. We show that the use of an un-analyzed detection makes the polarization-dependence read-out highly robust to scattering effects, even in regimes where imaging might be degraded. The effects are illustrated in polarization resolved imaging of myelin lipid organization in mouse spinal cords.

OCIS codes: (120.2130) ellipsometry and polarimetry; (120.5820) scattering measurements; (180.4315) nonlinear microscopy; (290.4210) multiple scattering; (290.5855) scattering, polarization; (290.7050) turbid media.

References and links

1. S. Brasselet, "Polarization-resolved nonlinear microscopy: application to structural molecular and biological imaging," Adv. Opt. Photon. **3**, 205–271 (2011).
2. P. Stoller, B. M. Kim, A. M. Rubenchik, K. M. Reiser, and L. B. Da Silva, "Polarization-dependent optical second harmonic imaging of a rat-tail tendon," J. Biomed. Opt. **7**, 205–214 (2000).
3. R. M. Williams, W. R. Zipfel, and W. W. Webb, "Second-harmonic generation images of collagen I fibrils," Biophys. J. **88**, 1377–1386 (2005).
4. S. Psilodimitrakopoulos, S. I. C. O. Santos, I. Amat-Roldan, A. K. N. Thayil, D. Artigas, and P. Loza-Alvarez, "In vivo, pixel-resolution mapping of thick filaments' orientation in nonfibrilar muscle using polarization-sensitive second harmonic generation microscopy," J. Biomed. Opt. **14**, 014001 (2009).

#232579 - $15.00 USD Received 22 Jan 2015; revised 12 Mar 2015; accepted 15 Mar 2015; published 31 Mar 2015

5. J. Duboisset, D. Aït-Belkacem, M. Roche, H. Rigneault, and S. Brasselet, "Generic model of the molecular orientational distribution probed by polarization resolved second harmonic generation," Phys. Rev. A **85**, 043829 (2012).
6. I. Gusachenko, Y. G. Houssen, V. Tran, J.-M. Allain, and M.-C. Schanne-Klein, "Polarization-resolved second-harmonic microscopy in tendon upon mechanical stretching," Biophys. J. **102**, 2220–2229 (2012).
7. K. Tilbury, C.-H. Lien, S. J. Chen, and P. J. Campagnola, "Differentiation of col I and col III isoforms in stromal models of ovarian cancer by analysis of second harmonic generation polarization and emission directionality," Biophys. J. **106**, 354–365 (2014).
8. C. Macias-Romero, M. E. P. Didier, V. Zubkovs, L. Delannoy, F. Dutto, A. Radenovic, and S. Roke, "Probing rotational and translational diffusion of nanodoublers in living cells on microsecond time scales," Nano Letters **14**, 2552–2557 (2014).
9. F. Tiaho, G. Recher, and D. Rouède, "Estimation of helical angles of myosin and collagen by second harmonic generation imaging microscopy," Opt. Expr. **15**, 4054–4065 (2007).
10. Y. Han, V. Raghunathan, R.-R. Feng, H. Maekawa, C.-Y. Chung, Y. Feng, E. O. Potma, and N.-H. Ge, "Mapping molecular orientation with phase sensitive vibrationally resonant sum-frequency generation microscopy," J. Phys. Chem. B **117**, 6149–6159 (2013).
11. A. Gasecka, T.-J. Han, C. Favard, B. R. Cho, and S. Brasselet, "Quantitative imaging of molecular order in lipid membranes using two-photon fuorescence polarimetry," Biophys. J. **97**, 2854–2862 (2009).
12. A. Gasecka, P. Tauc, A. Bentley, and S. Brasselet, "Investigation of molecular and protein crystals by three photon polarization resolved microscopy," Phys. Rev. Lett. **108**, 263901 (2012).
13. P. Ferrand, P. Gasecka, A. Kress, X. Wang, F.-Z. Bioud, J. Duboisset, and S. Brasselet, "Ultimate use of two-photon fluorescence microscopy to map fluorophores orientational behavior," Biophys. J. **106**, 2330–2339 (2014).
14. D. Oron, E. Tal, and Y. Silberberg, "Depth-resolved multiphoton polarization microscopy by third-harmonic generation," Opt. Lett. **28**, 2315-2317 (2003).
15. M. Zimmerley, P. Mahou, D. Débarre, M.-C. Schanne-Klein, and E. Beaurepaire, "Probing ordered lipid assemblies with polarized third-harmonic-generation microscopy," Phys. Rev. X **3**, 011002 (2013).
16. G. Bautista, S. Pfisterer, M. Huttunen, S. Ranjan, K. Kanerva, E. Ikonen, and M. Kauranen, "Polarized THG microscopy identifies compositionally different lipid droplets in mammalian cells," Biophys. J. **107**, 2230–2236 (2014).
17. H. Wang, Y. Fu, P. Zickmund, R. Shi, and J.-X. Cheng, "Coherent anti-Stokes Raman scattering imaging of axonal myelin in live spinal tissues," Biophys. J. **89**, 581–591 (2005).
18. E. Bélanger, S. Bégin, S. Laffray, Y. De Koninck, R. Vallée, and D. Côté, "Quantitative myelin imaging with coherent anti-Stokes Raman scattering microscopy: alleviating the excitation polarization dependence with circularly polarized laser beams," Opt. Express **17**, 18419–18432 (2009).
19. M. Zimmerley, R. Younger, T. Valenton, D. C. Oertel, J. L. Ward, and E. O. Potma, "Molecular orientation in dry and hydrated cellulose fibers: A coherent anti-Stokes Raman scattering microscopy study," J. Phys. Chem. B, **114**, 10200–10208 (2010).
20. F. Munhoz, H. Rigneault, and S. Brasselet, "High order symmetry structural properties of vibrational resonances using multiple-field polarization coherent anti-Stokes Raman spectroscopy microscopy," Phys. Rev. Lett. **105**, 123903 (2010).
21. F. Munhoz, H. Rigneault, and S. Brasselet, "Polarization-resolved four-wave mixing for structural imaging in thick tissues," J. Opt. Soc. Am. B **29**, 1541–1550 (2012).
22. G. de Vito, A. Bifone, and V. Piazza, "Rotating-polarization CARS microscopy: combining chemical and molecular orientation sensitivity," Opt. Express **20**, 29369–29377 (2012).
23. F.-Z. Bioud, P. Gasecka, P. Ferrand, H. Rigneault, J. Duboisset, and S. Brasselet, "Structure of molecular packing probed by polarization-resolved nonlinear four-wave mixing and coherent anti-Stokes Raman scattering microscopy," Phys. Rev. A **89**, 013836 (2014).
24. D. Débarre, N. Olivier, and E. Beaurepaire, "Signal epidetection in third-harmonic generation microscopy of turbid media," Opt. Express **15**, 8913–8924 (2007).
25. A. Ishimaru, *Wave Propagation and Scattering in Random Media* (Academic, 1978).
26. W. F. Cheong, S. A. Prahl, and A. J. Welch, "A review of the optical-properties of biological tissues," IEEE J. Quantum Electron. **26**, 2166–2185 (1990).
27. V. V. Tuchin, L. V. Wang, and D. A. Zimnyakov, *Optical Polarization in Biomedical Applications* (Springer, 2006).
28. H. C. Gerritsen and C. J. De Grauw, "Imaging of optically thick specimen using two-photon excitation microscopy," Microsc. Res. Techniq. **47**, 206–209 (1999).
29. A. K. Dunn, V. P. Wallace, M. Coleno, M. W. Berns, and B. J. Tromberg, "Influence of optical properties on two-photon fluorescence imaging in turbid samples," Appl. Opt. **39**, 1194–1201 (2000).
30. V. R. Daria, C. Saloma, and S. Kawata, "Excitation with a focused, pulsed optical beam in scattering media: Diffraction effects," Appl. Opt. **39**, 5244–5255 (2000).
31. M. Oheim, E. Beaurepaire, E. Chaigneau, J. Mertz, and S. Charpak, "Two-photon microscopy in brain tissue: parameters influencing the imaging depth," J. Neurosci. Meth. **111**, 29–37 (2001).

#232579 - $15.00 USD Received 22 Jan 2015; revised 12 Mar 2015; accepted 15 Mar 2015; published 31 Mar 2015

32. P. Theer and W. Denk, "On the fundamental imaging-depth limit in two-photon microscopy," J. Opt. Soc. Am. A **23**, 3139–3149 (2006).
33. C. K. Hayakawa, V. Venugopalan, V. V. Krishnamachari, and E. O. Potma, "Amplitude and phase of tightly focused laser beams in turbid media," Phys. Rev. Lett. **103**, 043903 (2009).
34. E. Chaigneau, A. J. Wright, S. P. Poland, J. M. Girkin, and R. A. Silver, "Impact of wavefront distortion and scattering on 2-photon microscopy in mammalian brain tissue," Opt. Express **19**, 22755–22774 (2011).
35. H. Dana and S. Shoham, "Numerical evaluation of temporal focusing characteristics in transparent and scattering media," Opt. Express **19**, 4937–4948 (2011).
36. S. P. Morgan, M. P. Khong, and M. G. Somekh, "Effects of polarization state and scatterer concentration on optical imaging through scattering media," Appl. Opt. **36**, 1560–1565 (1997).
37. C. K. Hayakawa, E. O. Potma, and V. Venugopalan, "Electric field Monte Carlo simulations of focal field distributions produced by tightly focused laser beams in tissues," Biomed. Opt. Express **2**, 278–299 (2011).
38. D. Aït-Belkacem, A. Gasecka, F. Munhoz, S. Brustlein, and S. Brasselet, "Influence of birefringence on polarization resolved nonlinear microscopy and collagen SHG structural imaging," Opt. Express **18**, 14859–14870 (2010).
39. I. Gusachenko, G. Latour, and M.-C. Schanne-Klein, "Polarization-resolved second harmonic microscopy in anisotropic thick tissues". Opt. Express **18**, 19339–19352 (2010).
40. O. Nadiarnykh, R. LaComb, P. J. Campagnola, and W. A. Mohler, "Coherent and incoherent SHG in fibrillar cellulose matrices," Opt. Express **15**, 3348–3360 (2007).
41. D. Débarre, W. Supatto, A.-M. Pena, A. Fabre, T. Tordjmann, L. Combettes, M.-C. Schanne-Klein, and E. Beaurepaire, "Imaging lipid bodies in cells and tissues using third-harmonic generation microscopy," Nat. Methods **3**, 47–53 (2005).
42. F. Munhoz, S. Brustlein, D. Gachet, F. Billard, S. Brasselet, and H. Rigneault, "Raman depolarization ratio of liquids probed by linear polarization coherent anti-Stokes Raman spectroscopy," J. Raman Spec. **40**, 775–780 (2009).
43. P. Schön, F. Munhoz, A. Gasecka, S. Brustlein, and S. Brasselet, "Polarization distortion effects in polarimetric two-photon microscopy," Opt. Express **16**, 20891–20901 (2008).
44. R. Richards and E. Wolf, "Electromagnetic diffraction in optical systems. II. Structure of the image field in an aplanatic system," Proc. R. Soc. London Ser.-A **253**, 358–379 (1959).
45. D. Bicout, C. Brosseau, A. S. Martinez, and J. M. Schmitt, "Depolarization of multiply scattered waves by spherical diffusers: Influence of the size parameter," Phys. Rev. E **49**, 1767–1770 (1994).
46. G. M. Hale and M. R. Querry, "Optical constants of water in the 200-nm to 200-μm wavelength region," Appl. Opt. **12**, 555–563 (1973).
47. G. S. He, H.-Y. Qin, and Q. Zheng, "Rayleigh, Mie, and Tyndall scatterings of polystyrene microspheres in water: wavelength, size, and angle dependences," J. Appl. Phys. **105**, 023110 (2009).
48. J. Schäfer, S.-C. Lee, and A. Kienle, "Calculation of the near fields for the scattering of electromagnetic waves by multiple infinite cylinders at perpendicular incidence," J. Quant. Spectrosc. Ra. **113**, 2113–2123 (2012).
49. S. Bégin, O. Dupont-Therrien, E. Bélanger, A. Daradich, S. Laffray, Y. De Koninck, and D. C. Côté, "Automated method for the segmentation and morphometry of nerve fibers in large-scale CARS images of spinal cord tissue," Biomed. Opt. Express **5**, 4145–4161 (2014).
50. F. C. MacKintosh, J. X. Zhu, D. J. Pine, and D. A. Weitz, "Polarization memory of multiply scattered light," Phys. Rev. B **40**, 9342–9345 (1989).
51. J. M. Schmitt, A. H. Gandjbakhche, and R. F. Bonner, "Use of polarized light to discriminate short-path photons in a multiply scattering medium," Appl. Opt. **31**, 6535–6546 (1992).
52. L. F. Rojas-Ochoa, D. Lacoste, R. Lenke, P. Schurtenberger, and F. Scheffold, "Depolarization of backscattered linearly polarized light," J. Opt. Soc. Am. A **21**, 1799–1804 (2004).
53. N. Ghosh, H. Patel, and P. Gupta, "Depolarization of light in tissue phantoms - effect of a distribution in the size of scatterers," Opt. Express **11**, 2198–2205 (2003).
54. T. Yasui, K. Sasaki, Y. Tohno, and T. Araki, "Tomographic imaging of collagen fiber orientation in human tissue using depth-resolved polarimetry of second-harmonic-generation," Opt. and Quant. Elec. **37**, 1397–1408 (2005).
55. T. Yasui, Y. Tohno, and T. Araki, "Determination of collagen fiber orientation in human tissue by use of polarization measurement of molecular second-harmonic-generation light," Appl. Opt. **43**, 2861–2867 (2004).
56. S. W. Chu, S. P. Tai, C. K. Sun, and C. H. Lin, "Selective imaging in second-harmonic-generation microscopy by polarization manipulation," Appl. Phys. Lett **43**, 2861–2867 (2007).
57. P. Refregier, M. Roche, J. Duboisset, and S. Brasselet, "Precision increase with two orthogonal analyzers in polarization resolved second harmonic generation microscopy," Opt. Lett. **37**, 4173–4175 (2012).
58. J. Zeng, P. Mahou, M.-C. Schanne-Klein, E. Beaurepaire, and D. Débarre, "3D resolved mapping of optical aberrations in thick tissues", Biomed. Opt. Express **3**, 1898–1913 (2012).
59. I. M. Vellekoop and A. P. Mosk, "Focusing coherent light through opaque strongly scattering media," Opt. Lett. **32**, 2309–2311 (2007).
60. S. M. Popoff, G. Lerosey, R. Carminati, M. Fink, A. C. Boccara, and S. Gigan, "Measuring the transmission matrix in optics: an approach to the study and control of light propagation in disordered media," Phys. Rev. Lett.

#232579 - $15.00 USD Received 22 Jan 2015; revised 12 Mar 2015; accepted 15 Mar 2015; published 31 Mar 2015

1. Introduction

Nonlinear microscopy (NM) offers a number of advantages over its linear counterpart including extended penetration depths, higher spatial and temporal resolution. Over the last decades, NM has proven itself a very powerful technique to study biological systems. Polarization resolved nonlinear microscopy [1] builds on the developments of NM with the advantage of evaluating the polarization-dependent nature of the nonlinear coupling between molecular assemblies and light. In particular, the read-out of the polarization dependence of generated nonlinear signals contains information on the orientational disorder of molecules within the focus, giving structural insights beyond the diffraction-limit. In the context of biological nonlinear imaging, several polarization resolved techniques have been developed in second-harmonic generation [2–9], sum-frequency generation [10], two- and three-photon fluorescence [11–13], third-harmonic generation [14–16] and Coherent Anti-Stokes Raman Scattering (CARS)/Four Wave Mixing (FWM) [17–23] to cite a few. Among these techniques, the CARS/FWM processes are the only ones allowing signals in isotropic media, thus providing a homogeneous local coherent source at the focus, a feature of paramount importance in the discussion that follows.

Biological samples are intrinsically heterogeneous structures in both chemical composition and physical properties. The variation of refractive index leads to degradations not only in the image quality (aberrations, scattering) but also in the polarization state (depolarization). Therefore, understanding the factors that lead to degradations aid in overcoming current limitations in microscopy, *e. g.* penetration/imaging depths. Given the complexity of biological systems, typical points that are raised and have no comprehensive answers are: *i*) the effect of the geometry (epi- vs forward-detected signals) for coherent scattering; *ii*) the effect of excitation fields depolarization and its effect on the non-linearly generated signals; *iii*) the impact of wavefront distortions on the point-spread function (PSF) and the polarization state for highly turbid regions; *iv*) the relation between imaging depth limits and specimen morphology. These points have an urgent need to be addressed because of their immediate relevance for nonlinear biological imaging. For example, in most biological system — thick specimens like brain, spinal cords, skin etc — only epi-detected signals are possible for imaging because of the strong diffusive scattering in forward direction geometry [24].

Amongst degradation mechanisms in imaging biological systems, the most relevant are birefringence and scattering. Even though these phenomena are intensively studied and relatively well understood [25–27], *their relation to imaging* is often lacking. To bridge this gap, a number of studies have addressed the effects of scattering on imaging quality [28–35], on polarization state distortions [36, 37] including birefringence [38, 39], on the imaging penetration depth [28, 31, 32], on the PSF quality [29, 30, 33, 34], as well as on the influence of epi vs. forward geometry efficiencies [3, 24, 40, 41]. Nonlinear microscopy overall encompasses many parameters, *e. g.* the interplay of different excitation/emission wavelengths, the efficiency dependence relative to the coherence length of the process and the role of coherent versus incoherent (single-event) scattering. While those effects can be introduced partially in phenomenological approaches [39, 40] to explain empirical observations, the specific nature of depolarization mechanisms affecting separately excitation and emission processes have not been elucidated yet, as well as the role of epi/forward geometry on polarization dependencies in PRNM.

In this study, we address this issue and the general problem of quantifying the influence of scattering on the polarization response of a nonlinear signal, by using a FWM/CARS signal to produce a local nonlinear probe deep inside a medium. This contrast is intrinsically efficient, does not require specific medium symmetry, and is moreover polarization-dependent with known characteristics in isotropic regions of a sample [42]. It can thus be advantageously used

#232579 - $15.00 USD Received 22 Jan 2015; revised 12 Mar 2015; accepted 15 Mar 2015; published 31 Mar 2015

to locally quantify the amount of depolarization for both excitation and emission lights (defined hereafter by the Degree Of Linear Polarization: DOLP) in adapted experimental configurations. These characteristics make FWM/CARS an interesting contrast as compared to SHG [39, 40], which requires a non-centrosymmetric arrangement of molecules to be analyzed and thus potentially suffers from added birefringence effects [38, 39], and to THG, which strongly depends on phase mis-matching conditions brought by interfaces [24].

After a description of observed polarization dependent nonlinear signal in a typical scattering biological medium (imaging of lipid orientational order in the myelin lipid sheath of a mouse spinal cord), we develop two different experimental layouts to extract separately the DOLP information on the excitation and the non-linearly generated photons. To understand the effects related to the medium scattering strength, the sample thickness and the epi/forward geometries, we use a model system composed of polystyrene beads. The analysis show that depolarization in turbid media is not only dependent on the size of the scattering centers, but also on the thickness of the system. It is demonstrated that excitation polarization is poorly affected, which is due to the longer wavelengths used but more importantly, to the fact that the nonlinear process acts as a filter for remaining coherent propagation. Emitted photons can however be strongly affected by depolarization for thick biological samples. We show that avoiding depolarized signal read-out can be done based on an un-analyzed detection, which provides similar amount of information in most of the molecular order studies in biology [1].

To shortly review the characteristic quantities involved in the multiple scattering regime, some essential definitions are given here. The scattering length l_s (or scattering mean free path) is related to the single-event scattering cross section — together with the number density of scatterers — and gives the characteristic length of the penetration depth for (ballistic) light. Relevant for the multiple scattering regime, the transport mean free path $l_s^* = l_s/(1-g)$, where g is the anisotropy factor, gives the characteristic length where directionality is completely lost with respect to the incoming original propagation direction. The introduction of these quantities are helpful to describe the separation between ballistic and multiple scattering regimes [25, 27].

2. Experimental details

We used two different setups for CARS microscopy in this work. The sources for the first setup are provided by the output of an optical parametric oscillator (Chameleon OPO, APE) pumped by a Ti:Sapphire laser (140 fs, 80 MHz, Chameleon, Coherent). The OPO outputs Pump ($\lambda_{\text{Pump}} = 831$ nm) and Stokes ($\lambda_{\text{Stokes}} = 1088$ nm) beams that are temporally and spatially overlapped, steered into an inverted microscope (Eclipse Ti, Nikon) and focused with a moderate numerical aperture (NA) objective (0.75 NA, 40x, Nikon). Images are acquired by scanning the beam with galvo scanners. The generated CARS signal is spectrally isolated with suitable filters and polarization selected with film polarizers (LPVIS100-MP, Thorlabs) before being detected by photomultiplier tubes (PMT, R9110, Hamamatsu). This setup is used for the results presented in Figures 1, 2 and 4. A second setup, equipped with both forward and epi detections, is used in the remaining figures, and its thorough description can be found elsewhere [21]. Briefly, two electronically synchronized oscillators (76 MHz, Mira, Coherent) are used as Pump (3 ps, $\lambda_{\text{Pump}} = 720$ nm) and Stokes (130 fs, $\lambda_{\text{Stokes}} = 903$ nm) sources for obtaining the FWM polarized response. They are steered into the microscope and focused with a moderate NA objective (0.6 NA, 40x, Olympus). An upper objective of higher NA (1 NA, water-immersion, 60x, Nikon) is used for detection in forward geometry. On both epi and forwards sides, the signals are polarization selected with film polarizers (LPV1-A, Thorlabs), spectrally isolated with suitable filters and focused into PMTs modules operating in photon-counting mode (MP 953, PerkinElmer). The 2PF images were acquired by raster-scanning the samples using only the Pump laser as the excitation. In both setups, Pump/Stokes polarization

#232579 - $15.00 USD Received 22 Jan 2015; revised 12 Mar 2015; accepted 15 Mar 2015; published 31 Mar 2015

states are rotated using an achromatic half-wave plate (AHWP10M-980, Thorlabs) set in a motorized rotation stage before the dichroic mirrors of the respective microscopes. The reflection of the incident beams on the dichroic mirrors is seen to only slightly modify the polarization state of the light, with no diattenuation and small ellipticity [43]. The intermediate NA objectives were chosen in order to reduce z-polarized excitation [44], and therefore neglected in the discussion that follows.

The scattering media used in these experiments were composed of either 3 μm or 0.13 μm diameter ($2a$) polystyrene beads (Invitrogen) with size parameters (ka) [45] of 17.3 and 0.8, respectively, defined at 650 nm using refractive index of Hale and Querry [46] and He *et al.* [47]. The scattering lengths l_s were adjusted by suitable dilution in agarose solution in order to mimic scattering lengths of biological samples [26]. The scattering lengths were determined by measuring the extinction of the Pump laser through a thin slab of the dispersions, with scattered light and ballistic light spatially isolated in the fourier space of the objective used for transmission [24]. We used the Beer-Lambert law, together with the measured thickness, to extract the extinction length from which we assume to be dominated by scattering. For the small particle system, after determining the scattering length at the Pump wavelength, we rescale to the measured nonlinear wavelength for the analysis using the correct scattering cross section obtained from a Mie-type code [48]. Typical scattering lengths were in the range 35-140 μm. Thick biological samples consisted of spinal cords extracted from adult wild type mice and post-fixed with 4% paraformaldehyde at 4°C overnight. On the following day, fixed tissues were washed in phosphate-buffer saline (PBS) several times before being cut into $\approx$ 4-mm-long segments, immobilized in 3% agarose for preservation of specimens, then finally mounted in a petri dish. The thin specimens were prepared in a similar way, as described thoroughly in Bégin *et al.* [49], and consisted of cross-sectional 30 μm-thick acute slices extracted from dissected mice spinal cords. The slices were sealed between two coverlips filled with PBS solution. All experiments were performed at 21°C.

The degree of linear polarization (DOLP) used here is

$$\mathrm{DOLP} = \frac{I_{\parallel} - I_{\perp}}{I_{\parallel} + I_{\perp}}$$

where I denotes FWM/CARS intensity measured with an incident polarization either parallel ($\parallel$) or perpendicular ($\perp$) to the analyzed direction. In practice, the DOLP value is extracted from polarization dependences of the FWM/CARS signals with a varying α angle of the incident polarizations with respect to the horizontal axis in the sample plane [38]. $I_{\parallel}$ and $I_{\perp}$ values are extracted from the intensity values measured at $\alpha = 0°$ and $\alpha = 90°$ respectively. We stress that in isotropic media, the obtained DOLP is not affected by polarization distortions occurring at the reflection on dichroic mirrors, because only at intermediate angles the polarization state of the excitation beams become elliptical [43]. We have verified this assignment by measuring the DOLP in the forward direction with a distortion-free Ag mirror replacing the dichroic.

Note that in some cases studied here, the experiments could have been equally performed using a linear optical process. The advantage of using nonlinear processes is due to the very local response of the system behaving as quasi-point sources. This is particularly relevant when evaluating the excitation fields along the z-direction since a linear source within a scattering medium would behave as a large wide field (a speckle) excitation. A second aspect is that the evaluation is done at the wavelength of interest.

#232579 - $15.00 USD Received 22 Jan 2015; revised 12 Mar 2015; accepted 15 Mar 2015; published 31 Mar 2015

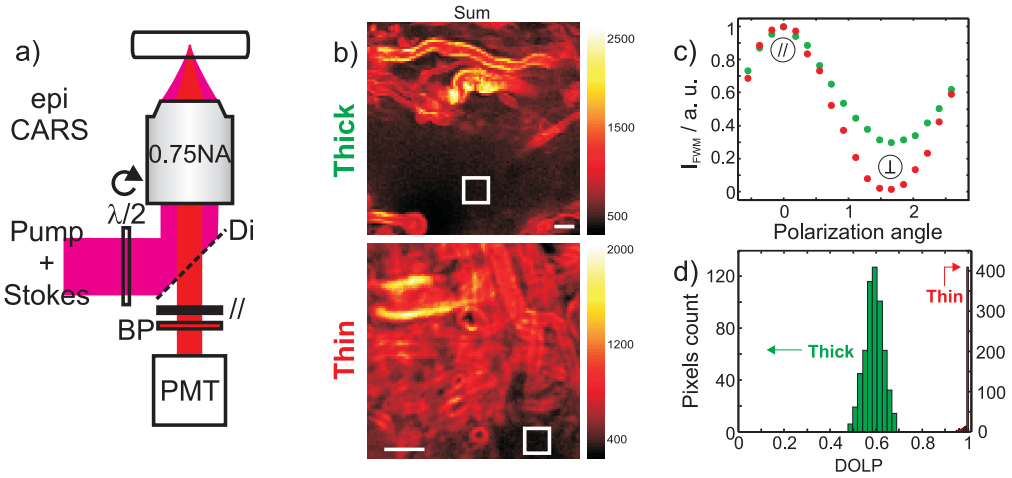

Fig. 1. a) Simplified experimental layout. Pump/Stokes beams are steered into an inverted microscope system and CARS photons are collected in the backward direction (epi geometry), polarization selected with analyzer (||) and spectrally filtered with suitable bandpass filter (BP) before detectors (PMT). b) epi-CARS images at the surface of a large and thick spinal cord (upper panel) or of a thin slice (lower panel). These images are generated by adding images taken at different excitation polarizations angles. c) Polarization responses from homogeneous regions in the background of the image, coming from non-resonant signal (FWM) from the isotropic surrounding medium of the myelin sheath fibers. Regardless of the homogeneous region probed, the polarization responses features are correlated with the length of the specimen. The intensity scale is normalized and the plots are the average of the pixels shown in the rectangle in part b). d) Quantified DOLP in both cases, on a region containing ≈100 pixels depicted by the square added in b). The scale bar is 5 μm.

3. Results and discussion

3.1. Evaluating the degree of depolarization in epi-imaging in a biological medium

Figure 1(b) shows epi-CARS images of a region in a whole spinal cord (thick) or in a cross-sectional slice (thin), taken close to the surface of the specimens. The images shown in Fig. 1(b) (and also in the figure of Section 3.4) are a sum of 18 images taken at excitation polarization angles in [0-π] range (step size is $\pi/18$). Typical penetration depths are 18 ± 2 μm for the two samples shown. The CARS wavelengths are chosen such as to target the chemical CH stretches present in lipids (centered at 2845 cm^{-1}), which form a dense layered membrane structure around axons named myelin sheath, visible as bright sections on the images. Inside the myelin sheath, the lipids are known to be radially oriented and ordered, giving rise to a non-trivial polarization response depending on the orientation and extent of disorder in their averaged orientational distribution [17, 18, 22, 23], which is discussed below in more detail. In contrast, a centrosymmetric medium such as found in the homogeneous, lower intensity regions of Fig. 1(b) (white rectangles) exhibits a known polarization response, as detailed in Munhoz *et al.* [42]. The signal in this region of the sample obviously come from non-resonant FWM responses, most likely from isotropic assemblies of proteins and the fixing agent (solvent). Even though this signal is weaker than a resonant CARS, it is still efficient and exploitable, which is a general feature of FWM/CARS imaging in tissues. The way the FWM polarization response projects on a given analyzer direction is characteristic of depolarization mechanisms of both excitation and emitted fields. To extract this information, we investigate here the FWM po-

#232579 - $15.00 USD Received 22 Jan 2015; revised 12 Mar 2015; accepted 15 Mar 2015; published 31 Mar 2015

larization dependence projected on the $\|$ analyzer direction (along the $\alpha = 0^\circ$ direction) and measure the DOLP value as defined above. In a scattering-free medium, a highly contrasted polarization dependence is measured with $I_\perp = 0$, leading to DOLP = 1, as expected from the FWM polarization response of an isotropic non-resonant medium [42]. In a scattering medium, the depolarization degree on the excitation field potentially degrades the contrast of this polarization response, decreasing the DOLP value. Similarly, depolarization of the emitted photons leads to a decrease of the DOLP value. In what follows, we assume that the excitation field DOLP is poorly affected by depolarization, given the fact that the focal spot is close to the surface of the sample, and further ascertained below in section 3.5. Consequently, the measured DOLP directly relates to the degree of depolarization affecting the emitted photons in the epi direction.

We observe that the polarization responses measured in isotropic non-resonant regions of spinal cord samples clearly depend on the extension of the scattering media. The thin sample shows a higher contrast in its polarization response (Fig. 1(c)) with a very narrow distribution around DOLP ≈ 1 (Fig. 1(d)). In contrast, the thick sample gives a signature of a higher depolarization with DOLP ≈ 0.55, even though the nature of the generated photons at the focal spot is the same. Furthermore, birefringence on the non-linearly generated photons can be neglected as the origin of depolarization. We have independently evaluated birefringence (for details see Aït-Belkacem *et al.* [38]) finding values that do not affect the determined DOLP. The explanation of the observed features involves decoupling the sample thickness, scattering lengths, *g*-values, excitation and detected polarization states within a material that is highly heterogeneous. To understand the mechanisms leading to depolarization, we therefore use phantoms of polystyrene beads to mimic the scattering properties of the biological specimens and the imaging geometry in a controllable manner. We first investigate the effect of penetration depth in a scattering medium, then the effect of the sample thickness.

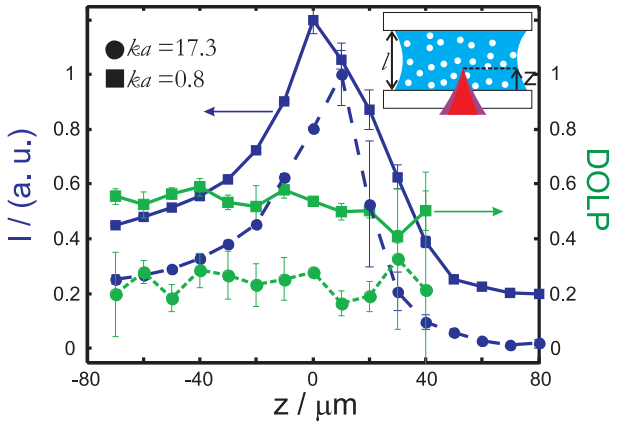

Fig. 2. Influence of scattering on the epi-detected FWM vs z-direction. The intensity measurements (blue) and DOLP measurements (green) are for different particles size systems: $ka = 17.3$, $l/l_s = 11$, $g = 0.83$ (dashed lines, circles) and $ka = 0.8$, $l/l_s = 9$, $g = 0.12$ (continuous lines, squares). The intensity raises as the focus reaches the glass-dispersion interface and after crossing it, drastically drops inside the scattering medium. Conversely, the DOLP is rather robust with a small slope. The intensity measurement for $ka = 0.8$ is shifted by 0.2 units for clarity purposes. Error bars are two standard deviation of three measurements (three non-resonant regions). The seemly missing error bars are smaller than the marker size.

#232579 - $15.00 USD Received 22 Jan 2015; revised 12 Mar 2015; accepted 15 Mar 2015; published 31 Mar 2015

3.2. *Influence on penetration depth*

Figure 2 shows the evolution of the DOLP and FWM intensity, measured in the epi-geometry, with the penetration depth into thick scattering phantoms of different natures. Overall, both DOLP and intensity depend on the morphology of the scattering centers. The intensity shows a non-monotonic behavior with the signal continuously increasing up to the glass-dispersion interface where it rapidly decreases. The increase is due to the residual reflected non-resonant signal plus the closer proximity of the objective focus to the source of multiply backscattered light [25]. The subsequent decrease arises from both spatial expansion of the excitation photons and loss of coherence due to strong wavefront aberrations [34]. Conversely, the DOLP is less sensitive to the penetration depth, but its value is dependent on the scatterer sizes. This behavior of the DOLP already suggests that the excitation field DOLP is not strongly affected, a point confirmed in section 3.5.

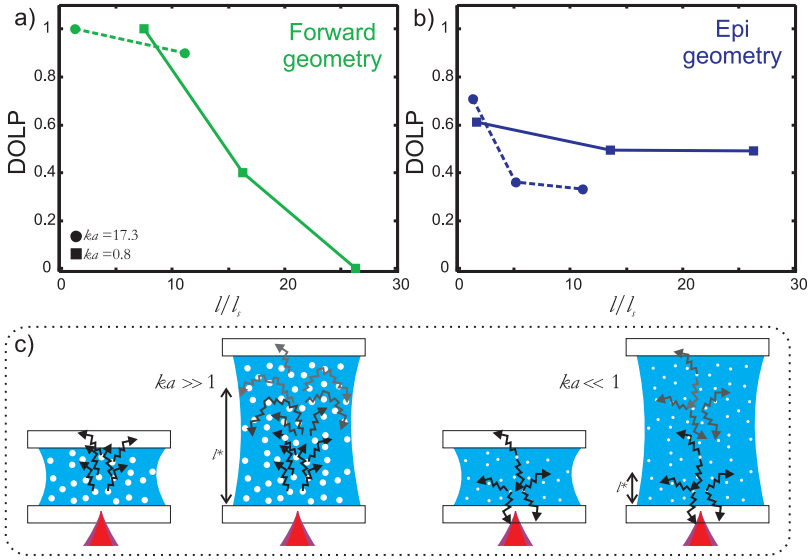

Fig. 3. Dependence of the depolarization of the detected photons on the (normalized) thickness of the scattering medium (l/l_s) and experimental geometry. a) DOLP of FWM photons detected in the forward direction (green) for particles smaller ($g = 0.14$, squares, continuous lines) and bigger ($g = 0.83$, circles, dashed lines) than the wavelength. b) Same as a), but in the epi direction. c) The panels depicts the depolarization mechanisms for each particle size used in this study (read text for further details). The features in the sketch are not in scale.

3.3. *Scattering of the non-linearly generated photons*

To investigate the effect of the system thickness, polarization responses are taken from photons generated from a centrosymmetric media (the lower glass slide, illustrated in the sketch in Fig. 3(c) at a distance of 100 μm below the glass-dispersion interface (no depolarization effects on excitation photons). Figure 3 shows the dependence of the DOLP on the thickness of the scattering media for both forward and epi direction geometries. We start with a discussion from the results in the forward direction geometry due to its more intuitive explanation. In the forward direction, scattering events for a media composed of large scattering centers (green dashed line in Fig. 3(a)) maintain a high polarization state purity even after many scattering events. This is remarkable given that the original ballistic photons have been attenuated by $\cong$ 11 orders of

#232579 - $15.00 USD Received 22 Jan 2015; revised 12 Mar 2015; accepted 15 Mar 2015; published 31 Mar 2015

magnitude. For small scattering centers (green continuous lines in Fig. 3(a)) the situation is different and the DOLP decreases at a much higher rate.

The behavior of the polarization state in the epi-direction is remarkably different (Fig. 3(b)). Regardless of the scatterer size, the DOLP does not change appreciably with l/l_s. There is always a decrease for both scatterer sizes, but for large scattering centers the decrease is more pronounced. These observations are in agreement with the results obtained for the biological samples. Overall, these results indicate that the DOLP in the epi-direction is a mixture of a single first scattering event together with multiply backscattered events. This is somewhat clearer for the large scatterers system where the interplay between a single scattering event (DOLP=1) at few l/l_s and multiple backscattered events at larger l/l_s contributes to a decrease in the DOLP. It is obvious, however, that for larger thickness, the "saturation" value of the DOLP strongly depends on the size of the scattering center.

The dependence of the polarization state through the medium is schematically depicted in Fig. 3(c). For scatterers much larger than the wavelength ($ka \gg 1$), the scattering pattern is highly anisotropic and most of the energy flux is forwardly directed. Therefore, many scattering events ($\approx l_s^*/l_s$) are needed to randomize the polarization state. Conversely, for small scatterers ($ka < 1$) the scattering pattern is almost isotropic and at a few scattering events the polarization state is randomized. More rigorously, the polarization state of the scattered photons shows a persistent polarization memory effect [50]: the polarization state of the scattered light is inherited from the excitation light. The strength of the polarization memory effect is known to be *ka*- and geometry-dependent [45, 50, 51]. According to Bicout *et al.* for a plane-wave impinging on a plane-parallel slab geometry [45], the DOLP decreases exponentially within the scattering medium with a characteristic length $\xi \cong l_s^*$, valid for $l \gg \xi$. Our results agree qualitatively with this, since we observe higher DOLP for the longer l_s^* ($ka = 17.3$). In epi-direction there are less theoretical models to compare to, but according to Rojas-Ochoa *et al.* the DOLP decreases monotonously with *g*-values, however evaluated only for "infinite" thickness media [52]. These comparisons and reasonable agreement could be simply fortunate because of the different geometry of the models and our experiment which is not a plane-wave excitation in a plane-parallel slab geometry. For example, the values we obtain for the DOLP in epi-geometry are somewhat higher than the plane-wave excitation [52], suggesting that there are small deviations still to be accounted for.

Regardless of the quantitative comparison between ideal models and real imaging conditions, the phantoms do seem to predict the behavior of the DOLP of the spinal cord images. The DOLP of the spinal cord samples is $\cong 0.55$, a value that indicates that the system is composed of small scattering centers. However, spinal cords are made of polydisperse structure sizes (scattering centers) that range from small to large sizes compared to the wavelength. Therefore, the DOLP observed in epi-direction for the spinal cords is biased towards the behavior of small scattering centers [53]. Within the scattering medium, however, for a variety of biological systems, l_s^* is generally much bigger than l_s [26]. This suggests that depolarization by scattering within the medium is only appreciable for depths $\approx l_s^*$. For example, using the values of g and l_s of brain from Cheong *et al.* [26] $l_s^* \approx 2.5$ mm. A comparison with the values of Fig. 3(a) shows that a rather high DOLP can be attained after going through 1 mm of brain ($l/l_s \approx 6$)!

We can therefore conclude that the DOLP in PRNM depends on the geometry and scattering center morphology. Importantly, the nonlinear emitted signal in a biological sample can be strongly affected by emission depolarization even in thin samples made of small scatterers. Interpreting polarization responses using an analyzer at the detection, which has been used in many studies [3, 4, 21, 54–56], is therefore likely to lead to biased results. In the absence of diattenuation, a detection without analyzers can however solve this issue and leads to robust measurements, since *both* polarization states are depolarized at the same rate. This means that

#232579 - $15.00 USD Received 22 Jan 2015; revised 12 Mar 2015; accepted 15 Mar 2015; published 31 Mar 2015

any modulation observed in the intensity response upon rotation of the excitation polarization state arises solely from the very original source (the focus). An un-analyzed detection is known to be only slightly poorer in terms of precision for the estimation of the retreived parameters [57]. Furthermore, it is known to provide the same amount of information on molecular order than analyzed detections in simple systems out of resonances and of cylindrical symmetry [1, 5, 23], as often met in biological imaging.

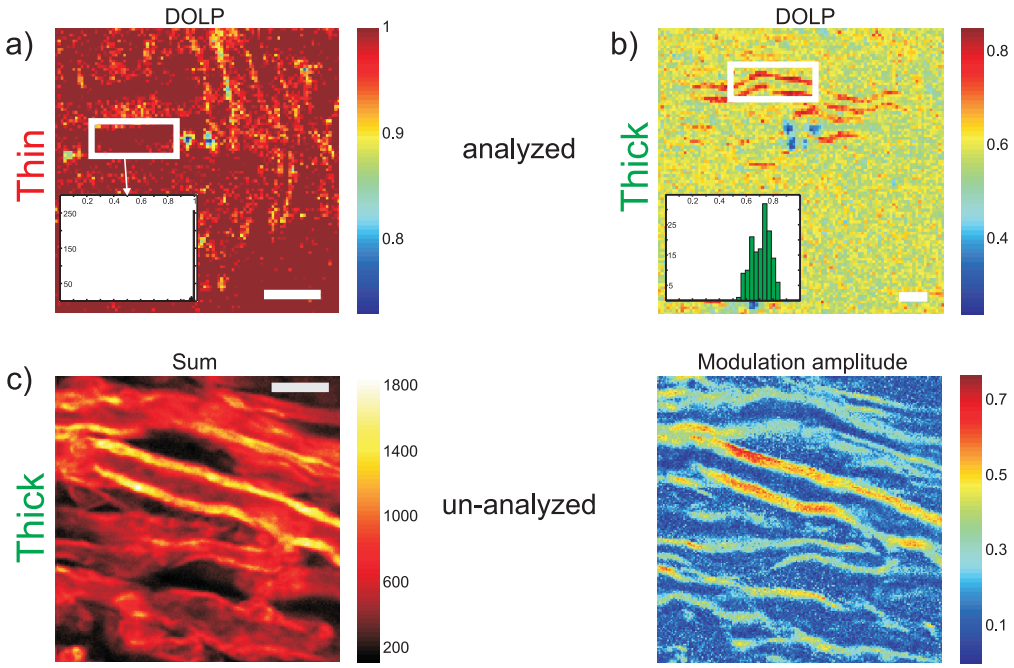

Fig. 4. CARS polarization dependence analysis in thick and thin spinal cord samples (see Fig. 1). a) DOLP images of the thin sample with histogram (inset) from horizontal fiber regions (white box). b) Similar analysis performed on the thick sample image. Note the disparate outcome when compared to part a), where aligned fibers and background have similar values. c) Similar analysis as in Fig. 1(b) (left panel) and Fig. 4(a),(b) (right panel) for a thick sample, but performed on data taken without any analyzer. Since the background does not have a modulation of the signal, it is filtered out from the analysis (right panel). We have also measured a thin sample in such experimental arrangement leading to similar results. The sum images should not be compared on a quantitative basis due to different experimental conditions. The scale bars are 5 μm.

3.4. Polarization resolved imaging in scattering biological samples

After exploiting polarization dependent FWM responses in isotropic media, we apply here the same methodology to investigate the influence of depolarization on polarization responses from ordered media in biological samples. A thorough description of the polarization response of organized lipids in the myelin sheath of axons can be found elsewhere [18, 22, 23]. Briefly, information on the molecular orientational distribution of active molecules (here CH stretching bonds of lipids measured by CARS microscopy) within the focus can be retrieved from a Fourier analysis of the CARS polarized response [23]. A strong modulated CARS polarization response is related to a strongly organized system, where molecules are highly packed and parallel. An orientational disorder lead to a decrease of contrast in the polarization modulation,

#232579 - $15.00 USD Received 22 Jan 2015; revised 12 Mar 2015; accepted 15 Mar 2015; published 31 Mar 2015

which can be misinterpreted in the presence of depolarization.

As mentioned above, an analyzed polarization response detection may lead to erroneous conclusions. Figure 4(a),(b) shows CARS polarization responses in myelin sheaths measured in a thin and a thick spinal cord samples using an analyzed detection (the sum of all polarization angles images is shown in Fig. 1(b)). For comparison, a similar measurement in a thick spinal cord is shown in Fig. 4(c), but without any analyzer. Fibers, with symmetry axis parallel to the analyzer direction, are expected to give an analyzed polarization response similar to that of an un-analyzed detection (compare Fig. 1(b) and images of Fig. 4(c) left panel). Therefore we chose to investigate the DOLP (identical to the polarization modulation amplitude) in horizontal fibers only. For thin samples, the DOLP of the fibers is comparable with the isotropic region (Fig. 4(a)), as expected from ordered molecules which would privilege nonlinear coupling along the $\parallel$ direction. Note that fibers in the $\perp$ direction exhibit a lower DOLP, which is expected since they create an anisotropic response along the $\perp$ direction. However, the DOLP is lower in the thick sample (Fig. 4(b)), which is a consequence of the presence of a higher depolarization, and therefore of a serious source of bias in the interpretation of polarization resolved data. The modulation amplitude measured in Fig 4(c) for fibers aligned along the horizontal direction corresponds to molecular angular apertures of about 120° to 140° along the $\parallel$ direction, using an analysis similar to Bioud *et al.* [23]. With such distributions, the expected DOLP in a non-scattering medium for a vertical analyzer is 1, which is indeed observed in the thin spinal cord sample. The measured DOLP in the thick sample, which is clearly underestimated, corresponds to a leakage of more than 50% of the $\perp$ analyzed detection channel into the $\parallel$ channel. We have also measured a thin sample un-analyzed (not shown), and obtained similar modulation amplitude values as in Fig. 4(c) (right panel). Therefore, we can conclude that a reliable estimation of molecular orientation parameters, using epi-detection, is only free of spurious features if performed without any analyzer [5, 23]. Note in addition that this experimental scheme allows to measure modulation amplitudes and deduce molecular angular aperture information whatever the fiber orientation, since the detection does not privilege any preferential analyzed direction.

3.5. Scattering of the excitation photons

The above-mentioned arguments are true provided that the excitation photons do not undergo any depolarization mechanism. In this part we quantify this effect, in conjunction with the concomitant image degradation. The microscope imaging quality is first checked by imaging an isolated 200 nm-diameter fluorescent polystyrene bead (Invitrogen) deposited between two glass slides filled with water. Figure 5(a) shows the experimental layout used for evaluating both polarization state and the PSF at the focus. The FWHM of the beads profile extracted from the 2PF images was 500 nm from which we estimate the PSF of the microscope to be 460 nm (assuming a convolution of two gaussians), close to the diffraction-limit value for the system (420 nm).

Figure 5(b) shows two representative line profiles of the fluorescent beads measured after a scattering medium ($ka = 17.3$ and $l/l_s = 1.9$) and a clear medium (water). As it can be clearly seen, there is no observable degradation of the resolving power of the NM images up to this depth. This demonstrate that the scattered photons do not participate in the nonlinear process.

The perseverance of the microscope PSF to scattering is in striking contrast with previously reports [34], nevertheless in agreement with others [29, 30, 33, 37]. The source of discrepancy lies in the intrinsic structure of the media and is only related to refraction effects. Scattering media composed of a homogenous distribution of small scatterers distort the wavefront without strong spatial correlations. This results in a wavefront phase that contains high frequency with low amplitude. This refraction results in a weaker intensity at the focus because of the loss of

#232579 - $15.00 USD Received 22 Jan 2015; revised 12 Mar 2015; accepted 15 Mar 2015; published 31 Mar 2015

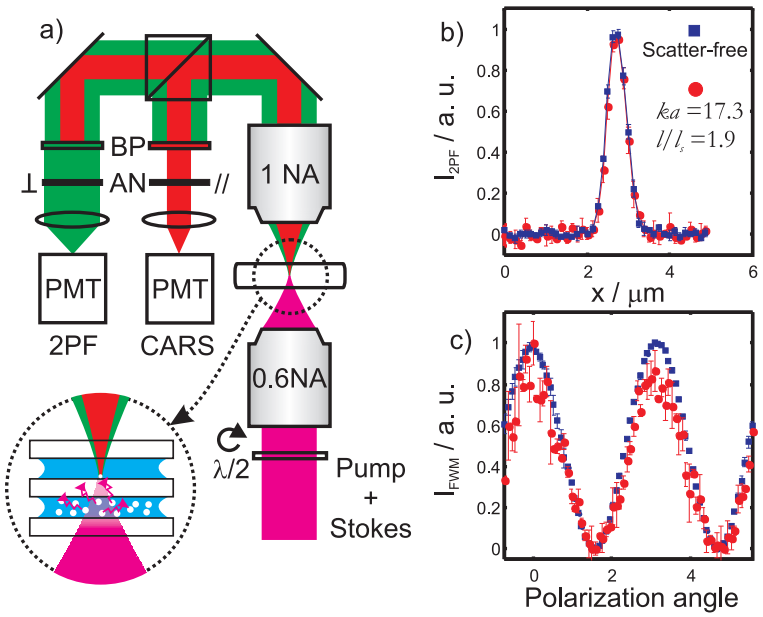

Fig. 5. Influence of scattering on image resolution (2PF) and depolarization of the excitation photons (FWM). a) Experimental layout for forward-direction experiments. To record the 2PF images, we blocked the Stokes beam to avoid any spurious processes. b) 2PF line profiles of a bead on a coverslip after a scattering medium ($g = 0.83$, red dots) and a transparent medium (blue square). The scattering medium length is 120 μm. One can obviously see that the resolution is not affected by scattering. Error bars are two standard deviation of three beads line profiles. c) FWM polarization responses generated after the scattering medium. Error bars are two standard deviation of two data sets.

coherence from different spatial frequencies [30, 33, 37]. However, the spatial frequencies are attenuated with equal weight and the resolution of the microscope is not affected.

Conversely, in the case of biological systems where long-range correlations exists, related to the mesoscopic structure of the specimens, the phase difference due to refraction among different spatial frequencies can achieve high amplitude [58]. This leads to loss of resolution and concomitant reduction of intensity at the focus. The resolution loss can be explained by using a superposition of different Zernike modes [34].

Our observation is further corroborated by the very high DOLP observed in the FWM polarization responses (Fig. 5(c)) taken in the same geometry. This shows in particular that in nonlinear processes within media that lacks diattenuation and birefringence, the degree of polarization is guaranteed before image degradation occurs, which was always observed at $l/l_s \leq 1$ in our experiments. Similarly as for the PSF preservation, this effect is mainly due to the fact that as long as coherence is preserved in the PSF formation at the focus, the DOLP is also conserved and the excitation photons, involved in the nonlinear optical coupling, appear therefore as non affected by depolarization.

4. Conclusions

We systematically quantified the effects of scattering on PRNM. We established that at imaging depths commonly accessible by PRNM, the polarization state of the excitation photons is preserved even though image resolution may be degraded. In respect to the nonlinearly generated

#232579 - $15.00 USD Received 22 Jan 2015; revised 12 Mar 2015; accepted 15 Mar 2015; published 31 Mar 2015

photons, regardless of the geometry, the DOLP depends on the size of the scattering centers and on the thickness of the specimens. For thick specimens, where forward direction imaging is not possible, the epi-detected DOLP is weakly dependent on the thickness, but depends on the size of the scattering centers: the larger the scattering centers the smaller the DOLP. Our discussion here holds for coherent scattering processes such as FWM/CARS, SHG and THG microscopy, provided that one rescales the characteristic lengths (l_s and l_s^*). These results show that PRNM in complex samples is possible, provided that an un-analyzed detection is used as demonstrated here for myeling sheaths in thick spinal cords. In particular, this gives a reliable and robust framework for future prospective studies in media of increasing complexity, such as buried regions of mice spinal cords and brains, that optical imaging is now reaching thanks to advances in wavefront shaping techniques [59, 60].

Acknowledgments

We thank F. Debarbieux and G. Rougon (Institut de Neurosciences de la Timone, Marseille, France) for providing fixed spinal cord tissue to visualize myelin sheath samples; Daniel Côté (Université Laval, Quebec, Canada) for providing the spinal cord samples; Naveen Balla, Patrick Ferrand, Carsten Cleff and Julien Duboisset for technical assistance with the CARS microscopes; Fatma-Zohra Bioud for fruitful discussions. This work has been supported by contracts ANR-10-INBS-04-01 (France-BioImaging infrastructure network), ANR-11-INSB-0006 (France Life Imaging infrastructure network), the A*MIDEX project (ANR-11-IDEX-0001-02) funded by the Investissements d'Avenir French Government program, managed by the French National Research Agency (ANR) and Conseil Régional Provence Alpes Côte d'Azur.

#232579 - $15.00 USD Received 22 Jan 2015; revised 12 Mar 2015; accepted 15 Mar 2015; published 31 Mar 2015